

## Full length Article

Sensorless full body active compliance in a 6 DOF parallel manipulator<sup>☆</sup>

Anirvan Dutta<sup>a</sup>, Durgesh Haribhau Salunkhe<sup>a</sup>, Shivesh Kumar<sup>b</sup>, Arun Dayal Udai<sup>c</sup>, Suril V. Shah<sup>a,1,\*</sup>



<sup>a</sup> Robotics Lab, Indian Institute of Technology, Jodhpur, India

<sup>b</sup> Robotics Innovation Center, German Research Center for Artificial Intelligence (DFKI GmbH), Bremen, Germany

<sup>c</sup> Autonomous Systems Lab, Birla Institute of Technology, Mesra, Ranchi, India

## ARTICLE INFO

## Keywords:

Parallel manipulator  
Sensorless active compliance  
Impedance control

## ABSTRACT

Parallel manipulators are being used extensively to cater to the needs of a multitude of industrial automation applications. Due to its kinematic accuracy and structural stiffness, parallel manipulators have proven considerable advantage over their serial counterparts. In modern applications, humans train, collaborate and interact with the manipulators in order to maximize the productivity and the quality of the final product. The critical factor in this human-robot interaction is safety and the ability of the mechanism to comply with human intentions. It thus becomes a necessity for the manipulator to detect external disturbances and interactions, and be able to react accordingly. In this research, a methodology for sensor-less full body active compliance is proposed on a 6-DOF RSS (Rotary-Spherical-Spherical) parallel manipulator. By using the proposed approach, the manipulator can detect and comply with the external forces on any part of its body without using any explicit force/torque sensor at the joint or the end-effector. This is done by utilizing the estimated joint torque based on the actuator current feedback only. A three-layer cascaded impedance controller for active compliance and reaction to various human interactions are reported. The proposed design and unique methodology for compliance exhibits an effective and inexpensive yet reliable alternative to be used in safe human-robot interactions and force controlled manufacturing applications.

## 1. Introduction

A parallel manipulator (PM) is a closed loop mechanism in which end-effector is connected with the base through several independent kinematic chains. PMs have structural stiffness and provide a higher load carrying capacity. In a PM, the error in the end-effector position due to backlash in the actuators do not add up as the number of actuators is increased leading to better kinematic accuracy compared to serial manipulators. Due to the compact design of PM, they can be mounted on a serial arm to extend their applications [1]. Hybrid serial-parallel manipulators have been developed to combine the advantages of serial as well as parallel manipulators and are used in industries as well as in academia [2–4]. Based on the advantages stated above, often for high payload applications and/or high speed tasks, parallel manipulators are preferred over serial arms. The DELTA + 1 DOF wrist robot [5] is being used extensively for fast pick and place operations in the food industry, manufacturing and assembling operations and 6 DOF

parallel manipulators have been considered for milling operations as well as high speed machining tasks [6–8].

These systems also find their application in the collaborative and domestic environment and operate along with humans thereby making their environment unstructured and dynamic. The innate nature of position controlled manipulators is to achieve a given task precisely without expecting a collision or interventions from human counterparts. Such position control strategies may be inadequate in the dynamic scenario because of their inability to accommodate errors and human uncertainties. Since safety is of prime importance in human-robot interaction applications, a different approach has to be taken to overcome the shortcomings of position-controlled strategies. Due to these reasons, there has been an increase in the research of compliant mechanisms [9,10], which facilitate these manipulators to handle human uncertainties and make them inherently safe for collaborative operations [11]. Force controlled strategies deal with the interactive forces and can detect an external disturbance during operation. Such

<sup>☆</sup> Conflict of interest: None.

\* Corresponding author.

E-mail addresses: [anirvan.dutta95@gmail.com](mailto:anirvan.dutta95@gmail.com) (A. Dutta), [salunkhedurgesh@gmail.com](mailto:salunkhedurgesh@gmail.com) (D.H. Salunkhe), [shivesh.kumar@dfki.de](mailto:shivesh.kumar@dfki.de) (S. Kumar), [arun\\_udai@bitmesra.ac.in](mailto:arun_udai@bitmesra.ac.in) (A.D. Udai), [surilshah@iitj.ac.in](mailto:surilshah@iitj.ac.in) (S.V. Shah).

<sup>1</sup> IIT Jodhpur

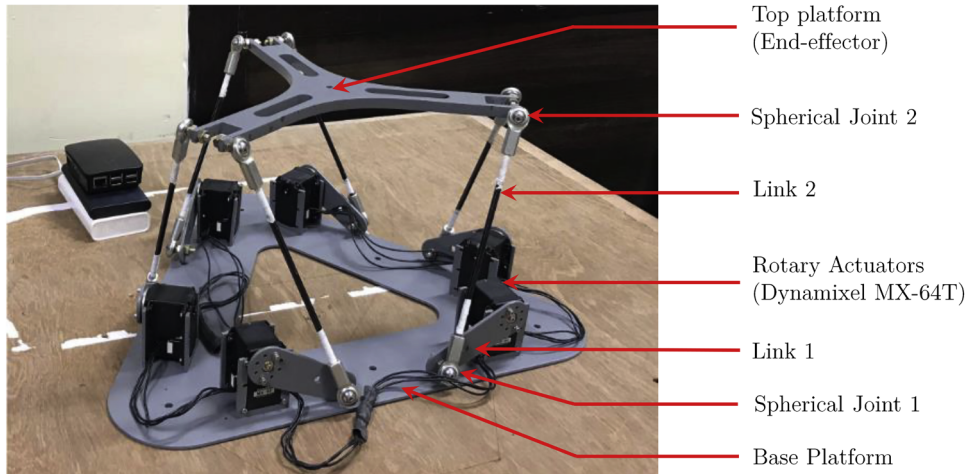


**Fig. 1.** The hardware setup of the proposed 6-DOF 6-RSS parallel manipulator.

strategies can be used where the expected interactive forces are known and some flexibility in the process is a must, one of such operations is an insertion task with low tolerances [12]. Force controlled manipulators are able to exhibit compliance and are able to collaborate with humans in an unstructured environment.

There are two types of compliance: i) passive compliance and ii) active compliance. The ability to conform to an external disturbance by the virtue of the flexibility of external springs or deformable links without using additional feedback is called passive compliance whereas the ability to sense external forces and react in a desirable manner is called active compliance. Passive compliant mechanisms are less complicated and are widely used where the torque requirements are within the limits of human capabilities [13,14]. On the other hand, active compliance has been proven better for a sophisticated task and heavy-duty operations [15,16]. Force feedback is required to achieve active compliance and to comply with variable stiffness. In most cases of active compliance, force/torque sensors are mounted at the end-effector, joints or base of the manipulator to carry out force-controlled tasks as well as to comply to the external forces [23,24]. The usage of sensors makes the detection accurate however, restricts the point of interaction or detection. Furthermore, joint torque sensors reduces the stiffness of the joints thereby limiting the payload capability of the manipulator and also limit the environments in which the manipulator can operate. To avoid the limitations of detecting external force through sensors, researchers have proposed and validated sensorless collision detection strategies in serial manipulators [17–20]. This method has been widely accepted, and many industries now implement such methods on serial manipulators for assembly and inspection tasks. Sensorless collision detection becomes an inexpensive add-on to the existing system and makes the manipulator naturally compliant and safe in human robot interaction scenario. It also overcomes the limit of detection area using external sensors. The robots which are already equipped with force/torque sensors at the end effector, sensor less collision detection techniques can be integrated as an additional safety check.

Compliant PMs can be used in operations where a large force is to be monitored such as surface finishing tasks, co-operative manipulation, assembly operations and human-robot interactions. These manipulators can also be used for tele-operations as they can provide applied force feedback data. Conventional manufacturing machines can be improvised with the force controlled parallel manipulators that are capable of multi-axis manufacturing. The advantages of a 6-DOF manipulator in additive manufacturing and spray-painting applications have been a focus of research [25,26] and with the presented research, the same versatility can be extended to traditional subtractive manufacturing. These manipulators can also be used where the environment is not known precisely, and it is desired for the manipulator to have

some degree of compliance. Force controlled assembly tasks are necessary where the task definition continuously changes and force feedback has to be used to perform the task satisfactorily [27]. The advantages of using 6-DOF parallel manipulators in exoskeletons and physical human interactions have been discussed in the recent years where active compliance is highly desirable [2,3,28,29].

**Contribution:** Passive compliance in PM has been reported several times in past research [14,30,31], but the area of sensorless active compliance in PM is very sparsely reported [21,22]. The idea of sensorless force compliance in [21] requires some prior knowledge about the end-effector in order to calculate the position and magnitude of the force. The paper discusses force compliance limited to any point on the end-effector only. Furthermore, it presents compliance to pure force and does not conclude about the compliance to rotational disturbances applied on the end-effector. The work in [22] is a recent one where the stiffness and position control are achieved independently for a PM. This research focuses on exploiting actuator redundancy to achieve active compliance and hence requires additional actuators and a modification in the manipulator design. In the proposed research work, we aim to address these shortcomings and present a full body active compliant 6-DOF PM as shown in Fig. 1. The paper presents a novel method of detection and compliance to an external force applied at any point on the moving part of the PM without using any external force/torque sensors. Instead, the approach utilizes an efficient implementation of the inverse dynamics model. Along with this, modified impedance control is presented for compliant motion control, as well as precise trajectory tracking. As a side contribution, we also present a comparison between two possible implementations of analytical inverse dynamics and choose the more efficient formulation for the real-time implementation as it is the bottleneck for the possible control loop frequency in the proposed framework. The presented methodology is generic enough and can be used for any parallel manipulator to implement active compliance. The presented work discusses a 6-RSS spatial manipulator to highlight the point that the active compliance can be achieved in all 6 degrees of freedom.

**Organisation:** The paper first discusses the geometrical and mechanical aspects of the manipulator and then presents the compliance strategy for the same. In Section 2, we present the design considerations and the configuration for the chosen PM to build a reliable, compliant system. This section discusses the manipulator architecture and its kinematic and dynamic modeling. It also discusses the advantages of the use of explicit loop closure functions and choice of the cut joints for dynamic analysis which leads to an efficient implementation for inverse dynamics. Section 3 explains the external force detection methodology and impedance control scheme for compliance. This section details the different scenarios considered for a compliant manipulator and its uses

in industrial as well as academic applications. Section 4 highlights the experimental set up for the compliant control implementation, presents the results and discusses the efficiency of the proposed framework.

## 2. Manipulator architecture and modeling

Various configurations and actuator options were considered while developing the necessary hardware for a compliant 6-DOF PM. Numerous results and findings have been reported earlier on the design of 6-DOF PM. Researchers have used linear actuators in 6 UPS (Universal-Prismatic-Spherical) [32,33] configuration and have implemented a design using rotary actuators in 6 RUS (Rotary-Universal-Spherical) [34] and 6 RSS (Rotary-Spherical-Spherical) [38,39] configuration. The advantages of the configuration and actuators chosen to build the PM is presented in this section.

### 2.1. Design considerations: actuation and configuration of the manipulator

Mechanisms developed by using rotary actuators have certain advantages over the mechanisms that use linear actuators. Use of rotary actuators, results in a lightweight design, facilitating the PM to be mounted on other devices as a force/torque sensor. The rotary actuators provide more flexibility regarding configuration, as links can be redesigned to produce different configurations with different kinematic and dynamic characteristics, whereas the mechanisms with linear actuators are mostly limited by their stroke length. Also, with the actuators at the base, a mechanism with lower mass-inertia can be developed which is suitable for the high-speed application.

The paper discusses sensorless collision detection and compliance, and thus force feedback was an important consideration while choosing the actuator. The proposed manipulator uses Dynamixel MX-64T motors from Robotis as shown in Fig. 1. The motor provides 6Nm stall torque and provides accurate proprioceptive (position and velocity) control through the Dynamixel embedded controller. The embedded controller provided real-time load, voltage and current feedback which was used for estimating torques at each actuated joint.

In past few years, various work has been reported in the field of kinematic and dynamic analysis of parallel manipulators [35–37]. There are mainly 3 types of design configurations reported for a 6-DOF PM with rotary actuators viz. the Hunt configuration [38], Zamanov configuration [39] and the Hexa parallel type [34]. The configurations are differentiated on the grounds of the placement of the rotary actuators which ultimately affects their kinematic as well as the dynamic characteristics. As discussed in [40], the Hexa parallel configuration has the largest workspace but poor global conditioning index (GCI) while the Hunt and Zamanov have better GCI at the cost of less volume of the workspace. As the aim of the compliant manipulator is to interact with the environment, the dynamic characteristics and global conditioning number were given preference over the workspace derived from the manipulator. The Zamanov type configuration was chosen (see Fig 1), and the link lengths were decided such that the workspace included a right circular cylinder with a diameter of 80mm and height of 100mm when the roll, pitch, and yaw angles are zero.

A 6-DOF manipulator was used with the objective of ultimately providing all the rotational and translation motions to the resulting system. The SS (spherical-spherical) pair used in the mechanism to join the link 2 with link 1 and the end-effector (ref Fig. 2) acts as a US (universal-spherical) pair along with an extra rotational DOF about the link 2 itself. As this extra DOF does not affect the pose of the end-effector, the manipulator can thus be treated as a 6-RUS system instead of a 6-RSS system for kinematic analysis as shown in the schematic diagram, Fig. 2. The manipulator has 36 joints including the 6 actuated joints and was separated into 6 independent subsystems. The inverse kinematic solution for the presented manipulator is discussed in the Appendix A.

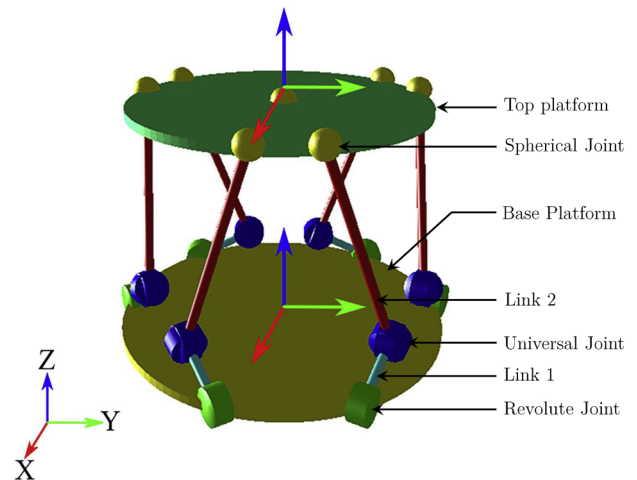
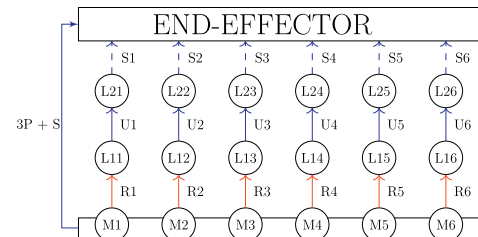
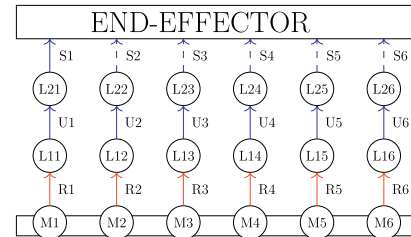


Fig. 2. Schematic of the parallel 6-RSS manipulator.



(a) Topological graph for the presented manipulator with end-effector attached with the base frame. In this case, joints S1 to S6 are the cut joints ( $n = 24$  and  $r = 18$ ).



(b) An alternate topological graph for the presented manipulator. In this case the end-effector is attached with the spherical joint S1 and joints S2 to S6 are the cut joints ( $n = 21$  and  $r = 15$ ).

Fig. 3. Topological representation: The red arrows represent actuated joints, the blue arrows are the passive joints and the blue dashed lines are the cut joints. (For interpretation of the references to color in this figure legend, the reader is referred to the web version of this article.)

### 2.2. Dynamic modeling

The two possible topological representations of the presented manipulator are shown in the Fig. 3. In the topological representation shown in Fig. 3a, the manipulator is cut open at all spherical joints, thus isolating the end-effector completely from the links. In this method, the end-effector is connected to the ground with 3 prismatic joints and a spherical joint as shown in Fig. 3a. In the topological representation shown in Fig. 3b, the manipulator is cut open at only five spherical joints, thus the end-effector is connected with one of the links using a spherical joint. It is important to note that the cut joints are passive in nature and only constraint torques are acted on the cut joints. In Fig. 3,

$M_x$  are the motors at the base while  $L_{1x}$  represents the first link of each subsystem and  $L_{2x}$ , the second link.  $R_x$ ,  $U_x$  and  $S_x$  are the revolute, universal and spherical joint representation respectively while  $P$  stands for the prismatic joint.

Consider a system of rigid bodies with  $N_B$  bodies,  $N_J$  joints and  $N_L$  kinematic loops. Let  $n = \sum_{i=1}^{N_B} n_i$  denote the degree of freedom of the spanning tree and denote the number of loop closure constraints. We have  $\mathbf{q} \in \mathbb{R}^{n \times 1}$ , consisting the active as well as the passive joint angle values required to define the end-effector and  $\mathbf{y} \in \mathbb{R}^{(n-r) \times 1}$ , stores the information of the position as well as the orientation of the end-effector.

As the inverse kinematics of the system is formulated initially, a unique mapping between the vector of joint angle values  $\mathbf{q}$  and the end-effector pose vector  $\mathbf{y}$  and can be mathematically expressed as,

$$\mathbf{q} = \gamma(\mathbf{y}) \quad (1)$$

The derivative and double derivative of Eq. (1) relates the angular velocities  $\dot{\mathbf{q}}$  and angular acceleration  $\ddot{\mathbf{q}}$  at joint level with the velocities  $\dot{\mathbf{y}}$  and acceleration  $\ddot{\mathbf{y}}$  of the end-effector, respectively.

$$\dot{\mathbf{q}} = \mathbf{G}\dot{\mathbf{y}} \quad (2)$$

$$\ddot{\mathbf{q}} = \mathbf{G}\ddot{\mathbf{y}} + \mathbf{g} \quad (3)$$

where,  $\mathbf{G} = d\gamma/d\mathbf{y}$ , is the loop closure jacobian matrix,  $\mathbf{G} \in \mathbb{R}^{n \times (n-r)}$  and  $\mathbf{g} = \dot{\mathbf{G}}\dot{\mathbf{y}}$ .

In closed loop systems, the equation of motion for a spanning tree of the system subjected to loop constraint forces can be given as:

$$\mathbf{I}(\mathbf{q})\ddot{\mathbf{q}} + \mathbf{C}(\mathbf{q}, \dot{\mathbf{q}}) = \boldsymbol{\tau} + \boldsymbol{\tau}_c \quad (4)$$

Here,  $\mathbf{I}(\mathbf{q}) \in \mathbb{R}^{n \times n}$  is the mass inertia matrix,  $\mathbf{C}(\mathbf{q}, \dot{\mathbf{q}}) \in \mathbb{R}^{n \times 1}$  is a vector of bias forces including Coriolis-centrifugal and gravitational forces,  $\boldsymbol{\tau}$  is the vector of torque variables while  $\boldsymbol{\tau}_c$  are the constraint forces produced by the cut joints. By using Jourdain's principle of virtual power (i.e.  $\mathbf{G}^T \boldsymbol{\tau}_c = 0$ ) and multiplying by  $\mathbf{G}^T$  on both sides of Eq. (4), the loop constraint forces  $\boldsymbol{\tau}_c$  can be eliminated.

$$\mathbf{G}^T \boldsymbol{\tau} = \mathbf{G}^T \boldsymbol{\tau}_{ID} \quad (5)$$

where,  $\boldsymbol{\tau}_{ID}$  is the inverse dynamics output of the spanning tree also stated as:

$$\boldsymbol{\tau}_{ID} = ID(\mathbf{I}(\mathbf{q})\ddot{\mathbf{q}} + \mathbf{C}(\mathbf{q}, \dot{\mathbf{q}})) = ID(\mathbf{q}, \dot{\mathbf{q}}, \ddot{\mathbf{q}}) = ID(\gamma(\mathbf{y}), \mathbf{G}\dot{\mathbf{y}}, \mathbf{G}\ddot{\mathbf{y}} + \mathbf{g}) \quad (6)$$

$$\mathbf{G}^T \boldsymbol{\tau}_{ID} = \mathbf{G}_u^T \boldsymbol{\tau}_{ID} \quad (7)$$

Here,  $\mathbf{G}_u \in \mathbb{R}^{(n-r) \times (n-r)}$  is a matrix containing rows of  $\mathbf{G}$  corresponding to the active joints while  $\mathbf{u} \in \mathbb{R}^{(n-r) \times 1}$  is the vector of actuator torques. For all non-singular configurations,

$$\mathbf{u} = \mathbf{G}_u^{-T} \mathbf{G}^T \boldsymbol{\tau}_{ID} \quad (8)$$

The use of explicit loop closure function is often inconvenient for the user, as it is not always possible to fulfill the condition for Eq. (1) and expressions for  $\mathbf{G}$  and  $\mathbf{g}$  are difficult to compute for a general case. In many cases, such as in the case of parallel manipulators, the advantages outweigh the manual effort needed to derive these functions because loop-closure errors cannot occur i.e.  $\mathbf{q}$  and  $\dot{\mathbf{q}}$  are obtained without integrating  $\ddot{\mathbf{q}}$  but are calculated by using Eqs. (2) and (3). This means that the loop constraints are analytically satisfied and there is no need for constraint stabilization terms [41,42].

Inverse dynamics of equivalent spanning tree of the manipulator was solved using the Rigid Body Dynamics Library (RBDL), an open-source C++ library that uses efficient  $O(n)$  Recursive Newton–Euler Algorithm (RNEA) for solving inverse dynamics of the tree type systems [43]. The spanning tree used to solve the inverse dynamics of the proposed manipulator uses 24 joints to constrain the manipulator and the topological representation has been illustrated in Fig. 3a. The 24 joints involve 3 joints ( $R + U$ ) of each leg and 6 virtual joints ( $3P + S$ ) used to constrain the end-effector. Another possible spanning tree exists in which the end-effector can be constrained through one spherical joint as shown in Fig. 3b. This representation consists of only 21 joints and

has no virtual joints involved. This method proved to be computationally more expensive while solving for the actuator torques as the rows of  $\mathbf{G}$  and  $\mathbf{G}$  corresponding to the last spherical joint contains lengthy symbolic expressions. In the analysis, it was found that the inverse dynamic computation of 24 joint solution (Fig. 3a) provided an execution rate of 500Hz on i5 4th Gen processor whereas, the 21 joint solution (Fig. 3b) provided 100Hz. Hence, the topology given in Fig. 3a was chosen for the real-time implementation of inverse dynamics routine, providing higher frequency of the cascaded controller described in the next section. Although both approaches have been independently reported in the literature of Multi-Body Simulation (MBS) and robotics, a direct comparison in the computation time has not been reported to the best knowledge of the authors. Hence, this finding constitutes a side contribution of this research work and it significantly affected the reaction time of the manipulator during compliance.

### 3. Sensorless compliance strategy

After the inverse dynamics is solved, it is critical to interpret the torque values from actuators and implement a control strategy for the compliance. To enable human-robot interaction, it is essential for the parallel manipulator to follow the human intention or comply with the external force. Various reaction strategies are reported in the literature for compliant control of the manipulators [44,45]. Among all these methods, impedance control strategy, which is an indirect force control methodology was chosen in this research because of its uncomplicated nature and efficiency in real-time control. In impedance control strategy, the behavior of the end-effector of the manipulator is modified to act as a spring, mass and damper system in the event of interaction, i.e., the mechanical impedance of the end-effector is regulated [45]. The desired impedance of the end-effector can be expressed as:

$$\mathbf{M}_d(\ddot{\mathbf{y}} - \ddot{\mathbf{y}}_0) + \mathbf{D}_d(\dot{\mathbf{y}} - \dot{\mathbf{y}}_0) + \mathbf{K}_d(\mathbf{y} - \mathbf{y}_0) = \mathbf{w}_e \quad (9)$$

Here,  $\mathbf{M}_d$ ,  $\mathbf{D}_d$  and  $\mathbf{K}_d$  are the diagonal matrices that include the desired inertia, damping and stiffness coefficients. The pose of the end-effector is represented by  $\mathbf{y}$ , as introduced in Section 2.2, and  $\mathbf{y}_0$  represents its initial value. The measured contact wrench at the end-effector is denoted by  $\mathbf{w}_e$ .

The use of impedance control can be justified in the case of compliance and safety, as when an external force is applied, the end-effector will deviate from its initial pose and follow the desired motion according to the external force. Impedance control scheme has been implemented in various forms depending on the measured input and desired output [45,51,52]. Implementation of traditional impedance control strategies have few drawbacks [46] since it directly controls the motor torque due to which it becomes essential to have an accurate inverse dynamic model, as well as precise information of the external force during the interaction. Further, the parameters  $\mathbf{M}_d$ ,  $\mathbf{D}_d$  and  $\mathbf{K}_d$  also control the trajectory tracking in the absence of external force and the selection of parameters becomes a challenging task. To overcome the above shortcomings of implementation of traditional impedance control, three layers cascaded control was proposed which modifies the impedance control scheme to control the force applied through the end-effector purely by motion control based on the scheme presented in [47]. There are two major components of the proposed sensorless compliance strategy, firstly the estimation of external wrench without the use of an external sensor and secondly, complying efficiently to the external wrench using a modified three layer cascaded controller.

#### 3.1. Estimation of external wrench

To implement the impedance control for active compliance, the detection of external disturbance is of utmost importance. The manipulator can be controlled efficiently if the external force applied to the manipulator is accurately estimated such that the Eq. (9) reflects as desired. The proposed formulation is able to provide full body

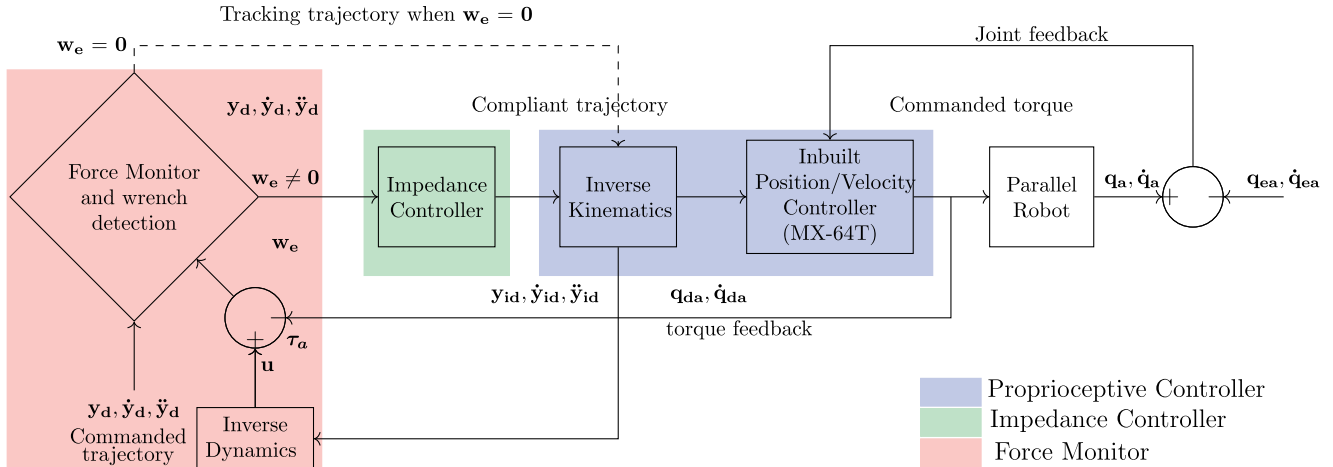


**Fig. 4.** Schematic diagram of 3 layer cascaded impedance control.

compliance which is discussed further.

It can be shown from the dynamic modeling of the manipulator that the external wrench,  $w_e = [f_x, f_y, f_z, m_x, m_y, m_z]^T$ , acted upon the end-effector can be related with the torques at the actuated joints as follows:

$$\mathbf{G}_u^T \tau_{diff} = \mathbf{w}_e$$

where,  $\tau_{diff} = \tau_{actual} - \mathbf{u}$  (10)

Here,  $(f_x, f_y, f_z)$  are the orthogonal components of force and  $(m_x, m_y, m_z)$  are the orthogonal components of moment in the external wrench.  $\tau_{actual}$  is the torque measured at the joint through the actuators at any given state of the manipulator while  $\tau_{diff}$  is the difference between the actual torque and the expected torques at the actuated joint as calculated from Section 2.2.

### 3.1.1. Force projection

This section discusses the challenges in making the manipulator full body compliant. It also presents a novel approach to detect and comply to an external force applied on any movable link of the manipulator. The method proposed in Section 3.1 can be used in operations where force is to be exerted through the end-effector. The research aims to make the manipulator compliant in such a manner that even if the system is disturbed at any movable point on the manipulator other than the end-effector, it should comply accordingly and so the following equation would suffice the purpose.

$$\mathbf{G}_{ux}^T \tau_{diff} = \mathbf{w}_x \quad (11)$$

Here,  $\mathbf{G}_{ux}$  is similar to  $\mathbf{G}_u$  at the point of application of external wrench,  $\mathbf{w}_x$  applied apart from the end-effector. From Eq. (11) it is clear that for full body compliance either  $\mathbf{w}_x$  should be known completely or the location at which the force is acted upon should be pre-determined to calculate  $\mathbf{G}_{ux}$ . As no external aid is used to determine the contact, calculating  $\mathbf{G}_{ux}$  is not possible. It may be noted, that even after the point of contact is determined it is computationally expensive to calculate  $\mathbf{G}_{ux}$  matrix in real time. For the reasons mentioned above, an alternative method was investigated which was computationally inexpensive and produced effective results.

Due to the closed kinematic loops present in PM, the effect of the wrench applied at any point of the manipulator is reflected in the torques of all 6 actuators. In non-singular configurations,  $\det(\mathbf{G}_u) \neq 0$  and so the system of linear equations presented in Eq. (10) has a unique solution. The  $\tau_{diff}$  measured after a disturbance is introduced at any point can also be achieved by transferring the force vector to the end-effector. This method has not been tested before for active compliance in PM and can be used to make parallel manipulators full body compliant.

$$\tau_{diff} = \mathbf{G}_{ux}^{-T} \mathbf{w}_x = \mathbf{G}_u^{-T} \mathbf{w}_e \quad (12)$$

The same  $\mathbf{G}_u$  matrix from Eq. (10) was used even though the point of application of the force was other than at the end-effector. By using this method, the external wrench applied at any point on the manipulator is projected onto the end-effector and thereafter comply to the projected wrench vector. As the end-effector follows the generated compliant trajectory due to the projected wrench vector, the point of contact also follows a path that complies with the actual external disturbance. The proposed method works well with PM as the effect of external disturbance is reflected in all the actuated joints of the spanning tree. It has been proved to be satisfactory in full body compliance of the manipulator, and the results have been discussed in the Section 4.

### 3.2. Controller scheme: 3 layer cascaded control

In this section, control scheme and compliance strategies used for the manipulator are discussed extensively. To achieve a fast compliant control loop, the controller was divided in 3 layers having different functionalities and control frequencies. The overall block diagram of the cascaded controller is presented in the Fig. 4. The controller is divided into 3 different layers: I. Proprioceptive controller:

For enhanced disturbance rejection an inner proprioceptive joint controller, using Proportional, Integral, Derivative (PID) control law for the position and angular velocity is proposed. The controller behavior was critically damped so that it was able to track the end-effector pose accurately without any oscillations. The controller acts as the innermost layer (see Fig. 4) along with the inverse kinematics block and is a joint level Single Input and Single Output system (SISO); therefore 6 independent control loops are used for each actuated joint. For any taskspace trajectory, the joint angles were computed using Eq. (1) and the joint velocities were computed using Eq. (2). Since the joint states corresponding to the actuators were required, a permutation matrix consisting of zeros and ones was used.

$$\mathbf{q}_a = \mathbf{Sq} \quad (13)$$

where,  $\mathbf{S} \in \mathbb{R}^{(6 \times 24)}$  is a permutation matrix and  $\mathbf{q}_a \in \mathbb{R}^{(6 \times 1)}$  are the actuated joint values.

As the proposed impedance control scheme utilizes indirect force control through this joint control loop, it was crucial for this controller to have an accurate and fast response.

#### II. Impedance controller:

The intermediate impedance controller portrayed the impedance behavior and played a role only during interaction by generating the desired impedance trajectory for the inner proprioceptive controller. The trajectory was generated by solving the second order non-

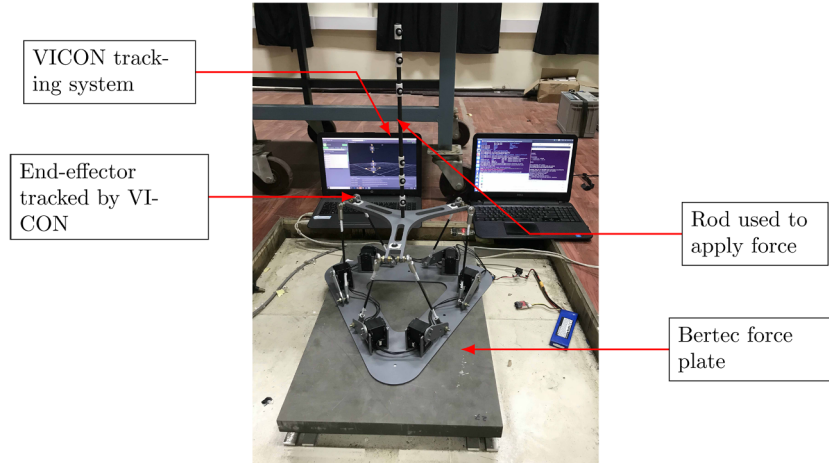


**Fig. 5.** Experimental setup for compliance control verification.

homogeneous differential Eq. (9) for real solutions of  $y$ . The derivation of the complete solution is presented in the Appendix B. Eq. (14) was analytically differentiated with respect to time for  $\dot{y}$ .

$$y_i = \frac{w_{ei}}{K_{di}} + c_{1i}e^{-(\lambda_{1i}t)/(2M_{di})} + c_{2i}e^{-(\lambda_{2i}t)/(2M_{di})} \quad (14)$$

where

$$\lambda_{1i,2i} = D_{di} \pm \sqrt{D_{di}^2 - 4K_{di}} \quad (15)$$

and  $c_1, c_2$  are constants to be determined based on condition before interaction ( $y_0, \dot{y}_0, \ddot{y}_0$ ). The term  $i$  varies from 1 to 6 corresponding to 6 taskspace variable i.e., 6 set of equations based on Eq. (14) are extracted. The  $i^{th}$  element of the calculated external wrench  $w_e$  is denoted as  $w_{ei}$ . The variables  $M_{di}, D_{di}, K_{di}$  are diagonal elements of the desired inertia, damping and stiffness matrices denoted by  $\mathbf{M}_d, \mathbf{D}_d$  and  $\mathbf{K}_d$  respectively.

During an interaction, the external wrench was calculated as described in the Section 3.1 and modified the impedance behavior of the point of application of the external wrench. The added advantage of such a scheme was that the parameters of the controller ( $\mathbf{M}_d, \mathbf{D}_d$  and  $\mathbf{K}_d$ ) could be modified to generate different impedance behavior without affecting the performance of the inner control loop. Therefore, independent stiffness, inertia and damping factor in all the 6 different task space direction could be maintained, conforming to the principle of active compliance.

### III. Force monitor:

The outermost layer of the control scheme was the force monitoring controller which sensed the feed forward term of the joint torques and regulated the impedance controller. It also computed the joint torques using the inverse dynamic formulation described the Section 2.2 in real-time for each joint state considering no external force. Based on the difference in the expected and actual joint torque, it switches the impedance controller on, or off and estimates the external wrench term in the event of compliance. Along with this, it also differentiates a collision from interaction by sensing duration of application of external force. If no external force was provided, it bypasses the impedance controller and provides the user-defined task space trajectory directly to the inner proprioceptive controller.

#### Implementation:

The inner proprioceptive controller formulated as the joint level SISO PID controller was inbuilt in the Dynamixel embedded controller, ensuring acceptable performance. The Software Development Kit (SDK) provided by the Dynamixel was utilised in interfacing with this controller at 10,000 baud rate. The outer impedance controller as well as the force monitor was implemented in C++ operating at a frequency of 500 Hz. C++ library, Eigen was utilised for efficient matrix

operations. The force monitor served as the primary control, which switched the trajectory generated for the inner controller to that of trajectory tracking or impedance control based on the feedback from the joints provided by the Dynamixel SDK.

The controller presented in the paper is hybrid in nature, i.e two continuous controller were triggered based on discrete events corresponding to when  $w_e = 0$  (no external force) and  $w_e \neq 0$ . To prove stability of such hybrid controller, a common Lyapunov based stability candidate can be employed based on [53]. As it is evident that the inherent controller of the framework is the position based PID controller, a Lyapunov candidate function formulated as given in [50] suffices the requirement. Based on [55], it can be proven that the position based PID controller is asymptotically stable. The proposed controller scheme makes the PM inherently compliant while maintaining the positional and taskspace accuracy. This scheme makes an important contribution in the control of PM, making it useful in industrial and domestic applications.

## 4. Results and discussion

In this section, the results and discussion of separate reaction strategies in the event of human interaction using sensorless compliance strategy is presented. The basis of these strategies lies in the sensorless estimation of the external wrench as well as kinematic and dynamic modeling of the PM. An experimental setup utilizing well calibrated systems such as Bertec® and Vicon® were used to verify the accuracy of the proposed methodology.

### 4.1. Experimental setup

As shown in Fig. 5, the designed and fabricated PM was attached on the top of Bertec® force plate system [54], which is an industrial force-torque sensor that measures three orthogonal components of the resultant force and moment applied on the plate. If any external force was applied to the manipulator, it was reflected by the force plate. Further, to verify the compliant motion, Vicon® motion tracking system [56] was utilized, which is a standardized 3D space localization system, utilizing 8 Motion Cameras along with infrared markers for tracking objects. Vicon® markers were fixed on the end-effector to track its trajectory during compliant motion. A vertical rod with two sets of Vicon® markers were utilized to precisely locate the force vector on the PM, in 3D space. Using the experimental setup in Fig. 5, different sets of the proposed sensorless compliance scheme was evaluated and validated.

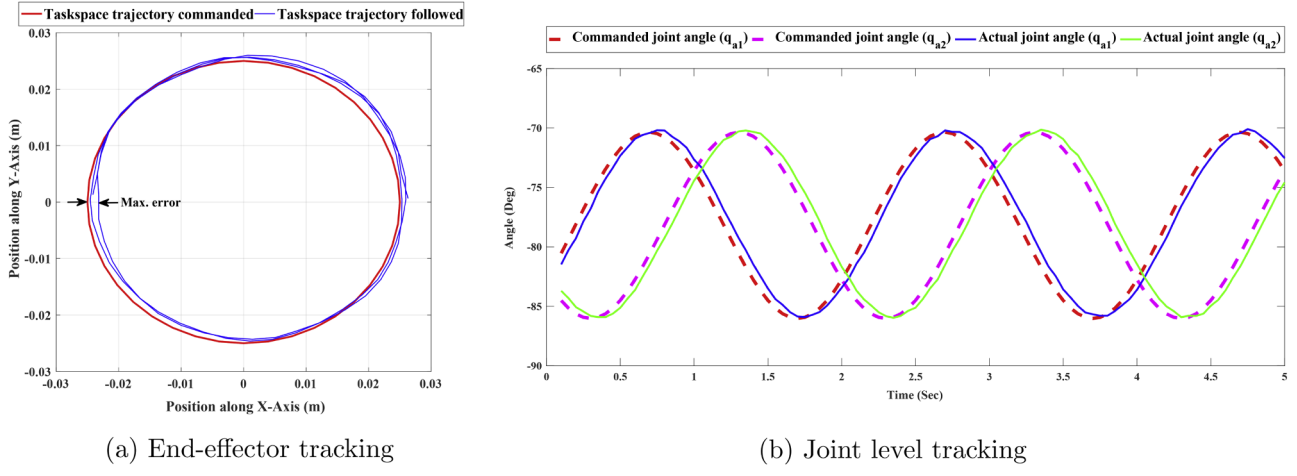


**Fig. 6.** Proprioceptive controller accuracy verified using VICON tracking for trajectory,  $x = 0.025\sin(2t)$ ,  $y = 0.025\cos(2t)$ ,  $z = 0.25$ . (For interpretation of the references to color in this figure legend, the reader is referred to the web version of this article.)

#### 4.2. Verification of inverse kinematic and inverse dynamic model

Different end-effector trajectories without external load were executed to check the accuracy of the kinematic as well as the dynamic model. Using the Vicon tracking, kinematic accuracy is presented in Fig. 6a which shows the comparison between commanded task space trajectory (shown in red) and trajectory followed by the end-effector (shown in blue). Fig. 6b shows the commanded joint angle and corresponding actual joint angles achieved by the joint actuators.

Verification of the dynamic model was not straightforward as the kinematic model, as no extrinsic joint torque sensor was used to provide the joint torques. Dynamixel motors MX-64T [57] provides current, voltage and load of the motor as feedback and after standard current-torque calibration technique, mapping of motor current to joint torques was used to estimate the actual joint torques. Fig. 7 shows the comparison between actual and theoretical joint torques for a user defined end-effector trajectory.

The results show that the PM was able to track the desired trajectory taskspace within 2% error thereby, confirming the accuracy of the kinematic model. Similar results were achieved for rotational motion and high-frequency trajectories. The torque plots show that, in high-frequency operation as shown in Fig. 7b, there was a considerable difference in the theoretical torques and actual torques. This may be due to high motor inertia terms and non-linear frictional terms which were not incorporated in the inverse dynamic model. Often these terms increase the complexity of the dynamic modeling and are computationally exhaustive. Another reason for this difference is the limitation of accurate current sensing capability of the Dynamixel motors. This leads to an important observation - the position based control will be more accurate than torque based

control. Therefore to achieve compliant behavior, position command based impedance control was used which utilized the inverse kinematic model of the PM in contrast to traditional impedance control which utilises torque commands from inverse dynamic model. However, to detect human interactions and estimate the external wrench, it was crucial to have correct theoretical torques. It was observed that the motor dynamics could be ignored in low-frequency operations and the proposed model works satisfactorily in such slow maneuvering as shown in Fig. 7a. The trajectory tracking error could be further minimized by precise manufacturing of the manipulator and by choosing actuators with low gear ratio and less backlash such as harmonic drive.

#### 4.3. Verification of sensorless compliance strategy

This section discusses various experiments implemented to verify the sensorless full body compliance strategy. The position control accuracy and torque comparison is shown in Figs. 6 and 7 and this section shows the verification of external force and compliant motion according to the disturbance. Human interaction could be accidental or intended, to demonstrate this, the results have been presented for both accidental collision and intended interaction for the purpose of active compliance. The proposed result presentation was motivated from [49].

##### 4.3.1. External wrench verification

External wrench estimation scheme was verified using Bertec<sup>®</sup> force plate system. The PM was locked at a fixed pose, and an external force was applied using the rod fixed at the end-effector. Readings from the force plate, as well as the estimated wrench, were compared. The plots in Figs. 8b and 9 b show that the proposed external wrench detection

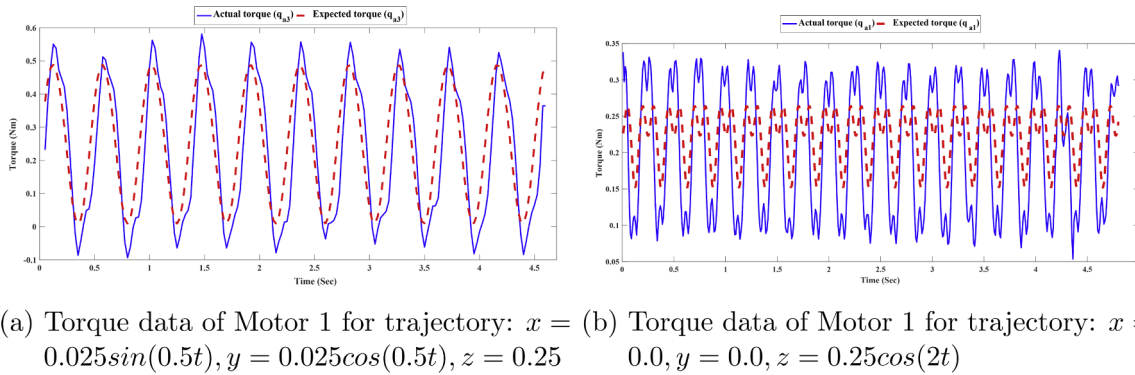


**Fig. 7.** Verification of inverse dynamic model.

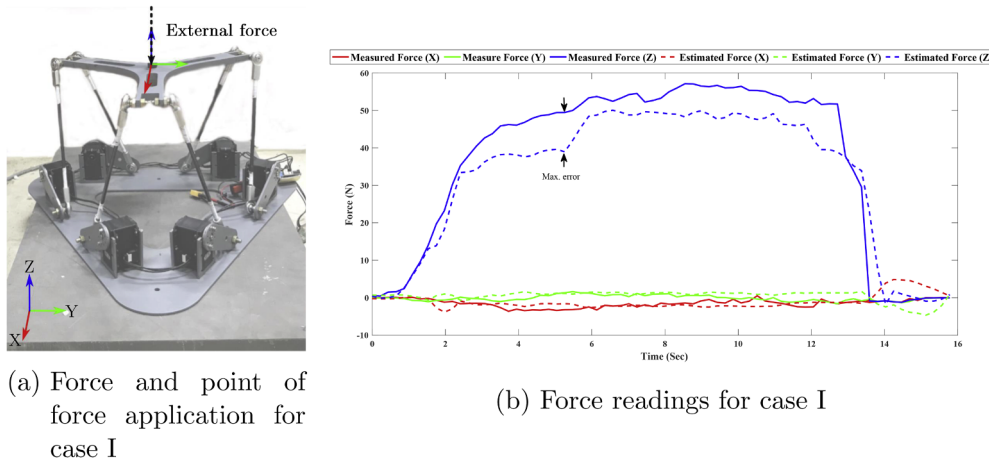


Fig. 8. Verification of Wrench detection using BERTEC force plate.

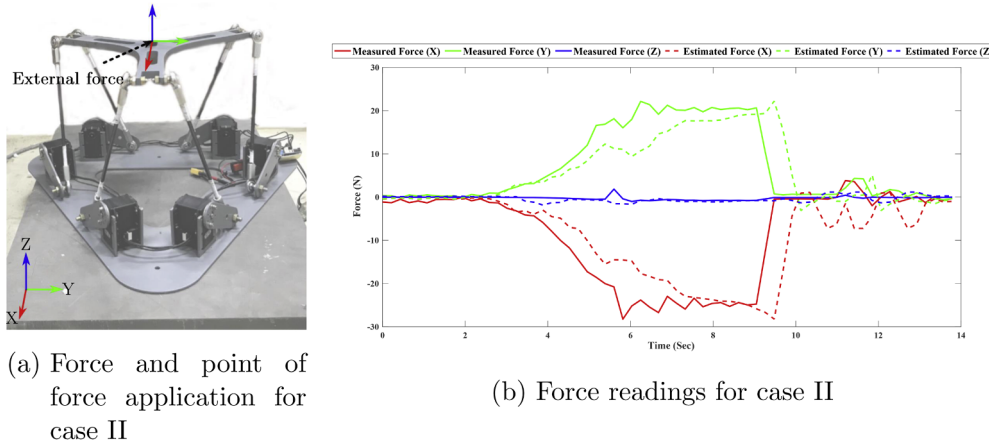


Fig. 9. Verification of Wrench detection using BERTEC force plate.

scheme has an error of less than 5% compared to standard force-plate measurement. Therefore, the PM can act as a light weight force feedback system and can be extended for haptic as well as tele-operations.

The accuracy of detection of the external wrench depends considerably on the performance of the hardware, specifically the actuators. Due to the high gear ratio of the Dynamixel motors, the accuracy of the wrench

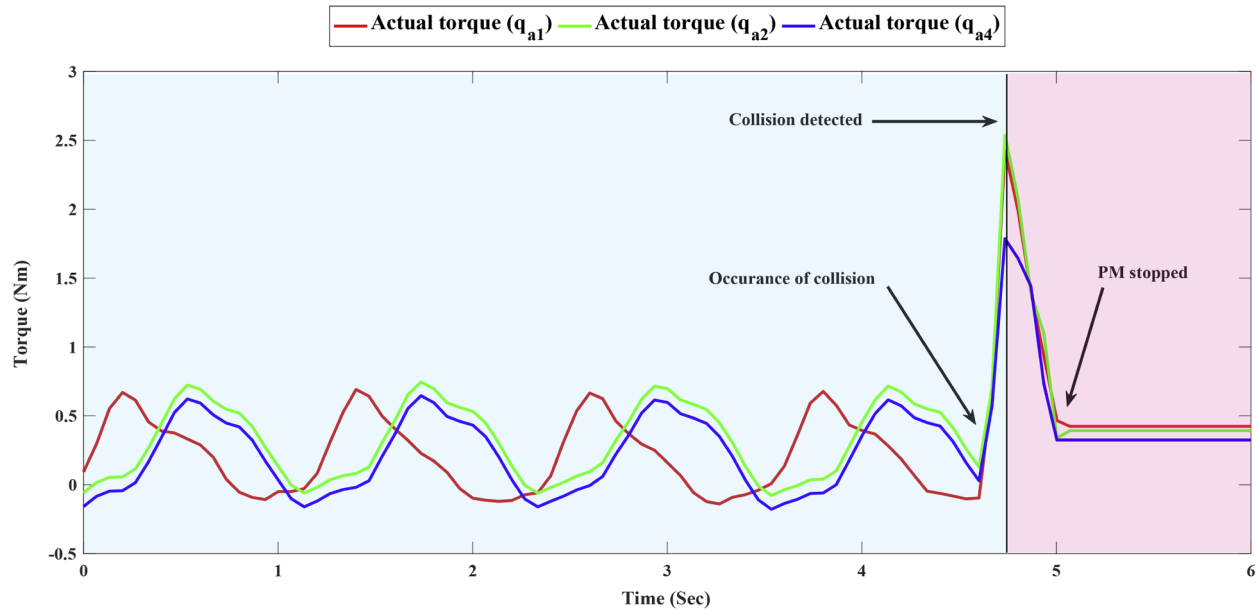


Fig. 10. Joint torque data during collision.

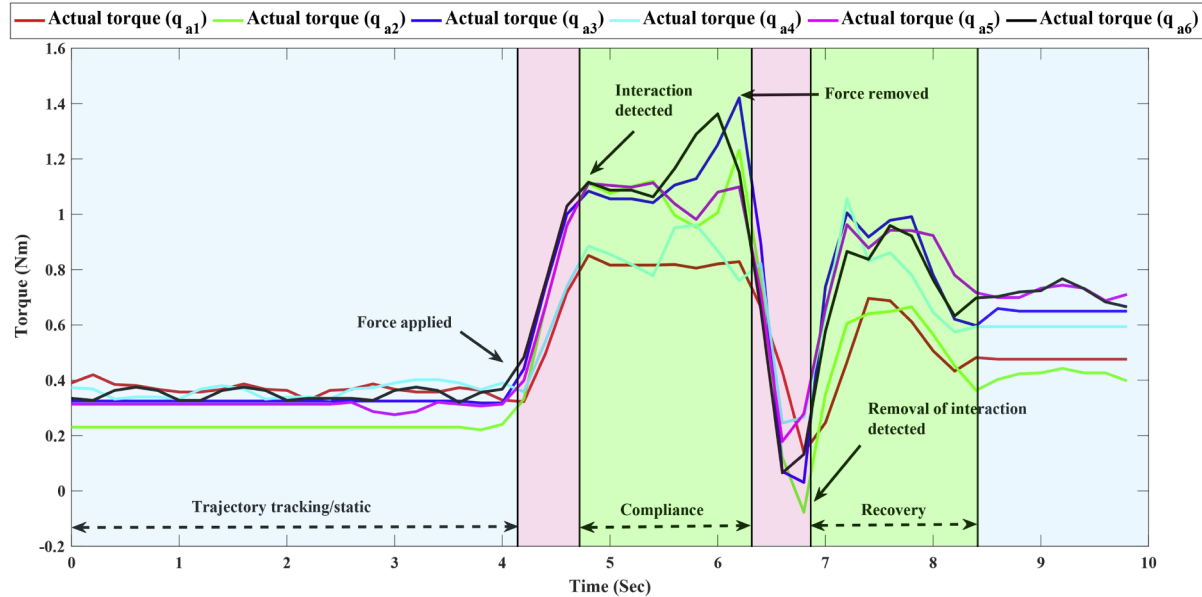
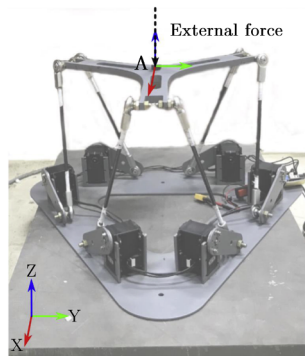


Fig. 11. Joint torques during compliant control.

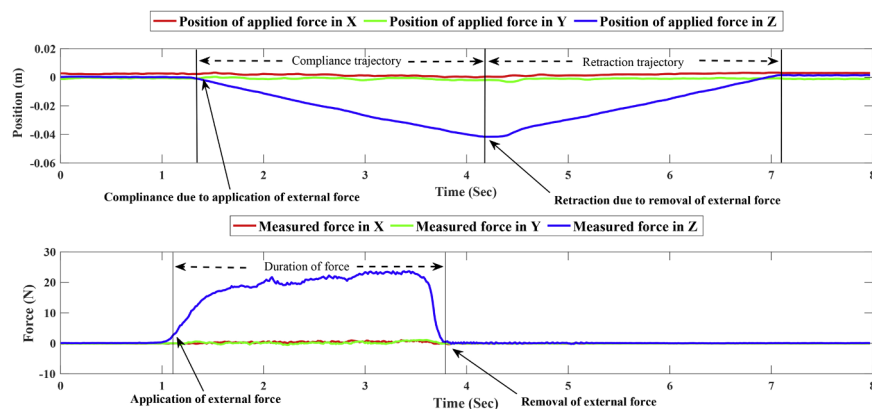
estimation was limited. Further, exhaustive current-torque calibration was not performed as it was beyond the scope of the paper. The mentioned factors can be accounted by using better hardware and the estimated wrench can be more accurate.

#### 4.3.2. Collision detection

When a collision occurs, the proprioceptive controller tries to avoid the joint error and increases the actuator torques, thereby creating a significant difference in expected and actual actuator torques. Such a



(a) Force and point of force application for Case I



(b) Compliance data from Vicon and Bertec force plate related to Case I

Fig. 12. Verification of compliant motion.

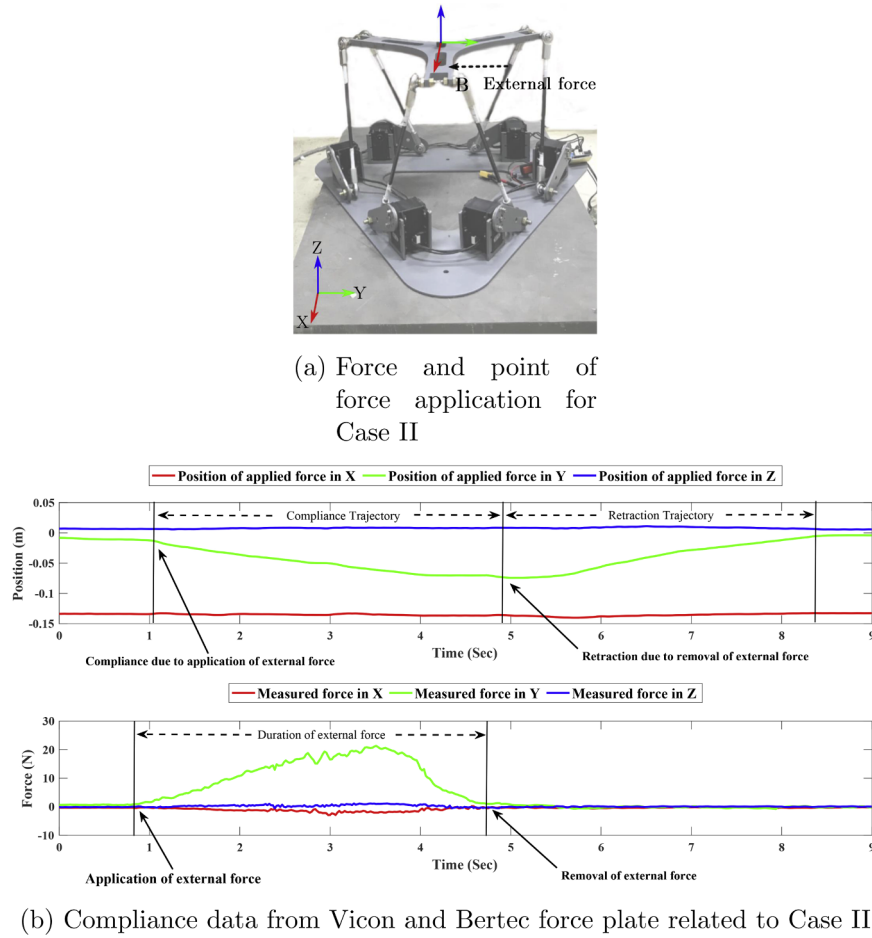


Fig. 13. Verification of compliant motion.

surge in torque difference was registered as a collision and the PM was stopped immediately at the current pose, and the joint torques were monitored for further intended collaborative motion by the force monitor layer. Fig. 10 shows the plot of actual joint torque during the event of a collision. To maintain clarity, only the torques of actuator 1, 2 and 4 are shown. At  $t = 4.75$ s, a collision occurred which suddenly increased the joint torques. The PM was stopped within 250ms and as the collision was removed, the actuators maintained a constant torque value suggesting a static position. By this experiment, the collision detection was successfully demonstrated. Based on our repeated experiments, it was found that the collision was detected within 300ms, which is considered acceptable based on the standards set in [48]. It may be noted the time required to detect collision was dependent on two factors, namely, the software framework which executes the methodology and the hardware framework which is provided in the Dynamixel SDK. The entire software framework was implemented in C++ to make it the efficient and time critical. However, the communication with Dynamixel SDK took place at 10,000 baudrate, this proved to be bottleneck of our detection time.

#### 4.3.3. Active compliance

If the external disturbance was acted upon the manipulator even after it stopped, the disturbance was registered as a case of intended interaction. For such incidence, the impedance controller was activated by the force monitor layer (refer Fig. 4). This results in complying with the end-effector in the direction of the applied force. This sequence is executed as long as an external force was detected, i.e., the difference between actual torques and estimated torques for any given joint state is beyond a threshold value. The threshold value was selected to avoid

the noisy jitters from Dynamixel motors. Due to the high gear ratio, the amplitude of the current feedback was quite low and was susceptible to noise. To avoid false detection, a threshold value was selected based on the minimum rise in current in the presence of human contact. Once the external force was removed, the impedance control generates the retracting trajectory such that the PM goes back to its original pose before the event of force application. Numerous experiments were conducted to validate the compliant motion. The Fig. 11 shows the actual actuator torques, during one such compliant motion when a vertical force was acted upon the end-effector of the manipulator. The plot can be grouped into four stages - 1) Initial stage of trajectory tracking or static case; 2) External force application and detection stage where sudden increase in the difference in the joint torques is measured and external wrench is calculated; A small time frame was kept to ensure the application of external force and avoid outliers. 3) Compliance stage, wherein the end-effector complies in the direction of applied force as long as the force is present and 4) Recovery stage, which starts after the force is removed, and the actual torques come close to the expected value. The PM recovers from the deflection caused by the applied force and goes back to its original state. Experiments for full body active compliance were carried out and validated by the precise tools available. The active compliance was tested when the force acted upon the end-effector as well as when it was applied on any other part of the manipulator. The following paragraphs discuss both the cases and present their results accordingly

Case I : *Compliant motion due to force at the end-effector* - Using the experimental setup as shown in Fig. 5, the accuracy of the compliant motion was verified by applying external force at end-effector. In Fig. 12a, an external force in negative z direction was applied at point A

using the rod. It becomes evident from Fig. 12b, that the end-effector, which was tracked by Vicon®, moved in the direction of the application of force and, as the force was removed it retracted back to its original state. The reaction time of the compliant motion was verified by the corresponding external force measured by the Bertec® force plate.

A small delay between the application of force and start of motion corresponds to a check described in the force monitor layer in Section 3.2, which differentiates collision and the intended interaction force.

**Case II : Compliant motion for force at the PM's body** To validate full body active compliance, a force along negative y direction was applied at point B which was not at the center of the end-effector as shown in Fig. 13a. In this case, the force was projected on the end-effector as discussed in the Section 3.1.1, and thereby projected compliant trajectory was generated. Tracking data from Vicon® of the point B shows that the compliant motion was along the direction of application of the force, which verifies the correctness of the proposed methodology. The measurement by the Bertec force plate confirms that compliant trajectory generated was according to the direction and magnitude of the external force applied at point B and adhered to the desired motion given by Eq. (9). The presented results confirm that the PM was able to comply to any external force applied to its movable part of PM's the body validating the proposed methodology for full body active compliance.

A [supplementary video](#) is also provided along with the text that demonstrates the different control strategies mentioned in the Section 3.

## 5. Conclusion

In this paper, a strategy for sensorless full body active compliant

## Appendix A. Inverse kinematics

In this section, we discuss the inverse kinematics solution of the presented manipulator. For the purpose of kinematic analysis, each subsystem was first transformed to a common frame and the angles related to the pose of the end-effector were calculated using geometric solution and the calculation is shown in the following section. As both, the input trajectory and the trajectory for compliance, are limited by the physical joint angle limits, the kinematic feasibility of the end-effector was a pre-check before complying along a trajectory.

Structure definition (refer Fig. 14):

- $l_1 \leftarrow$  length of the link coupled with second joint
- $l_2 \leftarrow$  length of the link coupled with third joint
- $\theta_{1i} \leftarrow$  Angle of Link 1 with respect to the x-axis in XZ plane
- $\theta_{2i} \leftarrow$  Angle of projection of Link 2 in XZ plane with respect to the extension of Link 1
- $\theta_{3i} \leftarrow$  Angle of Link 2 with respect to its projection in XZ plane
- $x_i, y_i, z_i \leftarrow$  The co-ordinates of the  $i$ th leg's spherical joint that is attached to the end-effector

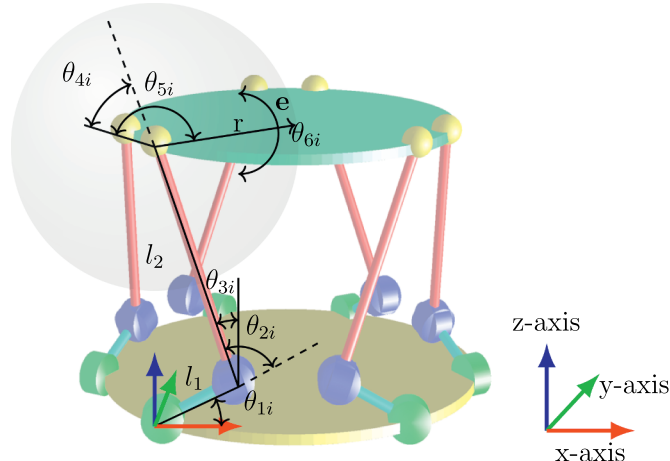


Fig. 1. Schematics explaining the joints of the subsystem.

parallel manipulator is developed which can be used in several industrial manufacturing applications. The novelty of our methodology lies in the ability to detect and actively comply to an external disturbance applied at any movable part of the parallel manipulator without the use of an explicit force/torque sensor. A three-layer cascaded controller was proposed for precise compliant motion as well as trajectory tracking. Trajectory tracking, force estimation and compliant motions are validated through various experiments. Separate strategy is presented for accidental collision as well as intended collaboration, thereby increasing the functionality of the proposed scheme. The accurate wrench detection at the end-effector makes the manipulator useful in all force controlled tasks such as industrial assembling, surface finishing, and cooperative manipulation as well as in the area of haptics and lead through programming. Due to its compact design it can also be used as a force/torque sensor mounted on a serial arm. The presented work can play an important role in cases of delicate operations or when unexpected human intervention is possible. The advantages of parallel mechanisms combined with the force sensing and control ability makes the presented manipulator safe, versatile as well as a competitive alternative to its serial counterpart. To the best knowledge of the authors, sensorless full body active compliance in a parallel manipulator has not been reported before.

## Acknowledgments

The authors sincerely thank Dr. Kaushal A. Desai, Assistant Professor, Department of Mechanical Engineering, IIT Jodhpur for discussions and insights on the manufacturing aspect of the mechanism in the early stage of this work.

The complete pose of the end-effector with respect to corresponding motor is known and given by  $[e, r]$  where  $e$  gives the position  $\{x_e, y_e, z_e\}$  and  $r$  provides information on the orientation {roll, pitch, yaw}. As the end effector is a rigid-body we can calculate the co-ordinates of all the spherical joints attached to the end-effector. The inverse kinematics is presented in a simplified manner by assuming a floating end effector. In this method we need to only calculate the 3 angles ( $\theta_{1i}, \theta_{2i}, \theta_{3i}$ ) related to the revolute and universal joint of each leg. The calculations related to the spherical joint ( $\theta_{4i}, \theta_{5i}, \theta_{6i}$ ) have been skipped here for brevity.

From geometry of the manipulator, one could derive all the necessary expressions:

$$\begin{aligned}\theta_{3i} &= \arcsin\left(\frac{y_i}{l_2}\right) \\ \cos(\theta_{2i}) &= \frac{x_i^2 + z_i^2 - (l_1^2 + (l_2 \cos(\theta_{3i}))^2)}{2l_1 l_2 \cos(\theta_{3i})} \\ \sin(\theta_{2i}) &= \pm \sqrt{1 - \cos(\theta_{2i})^2} \\ \theta_{2i} &= \arctan 2(\sin(\theta_{2i}), \cos(\theta_{2i})) \\ \theta_{1i} &= \arctan 2(z_i, x_i) - \arctan 2(l_2 \cos(\theta_{3i}) \sin(\theta_{2i}), l_1 + l_2 \cos(\theta_{3i}) \cos(\theta_{2i}))\end{aligned}$$

## Appendix B. Solution of second order non-homogeneous differential equation

[Eq. \(9\)](#) is a second order non-homogeneous differential equation with constant coefficients. In the scope of this work, the matrices  $M_d$ ,  $D_d$  and  $K_d$  are considered as diagonal and hence the solution presented here is provided with a scalar treatment representing the diagonal terms. Further, it is assumed that  $w_e$  is constant for a single interaction case. Performing a transformation on each scalar equation by taking  $y - y_0$  as  $y'$ ,  $\dot{y} - \dot{y}_0$  as  $\ddot{y}'$  and  $\ddot{y} - \ddot{y}_0$  as  $\ddot{y}''$  results into the following equation

$$M_d \ddot{y}' + D_d \dot{y}' + K_d y' = w_e \quad (16)$$

where,  $w_e \neq 0$ . The solution of the above equation can be expressed as

$$y' = y'_c + y'_p \quad (17)$$

where  $y'_p$  is particular solution and  $y'_c$  is the general solution of the corresponding homogeneous differential equation, given by:

$$M_d \ddot{y}' + D_d \dot{y}' + K_d y' = 0. \quad (18)$$

The solution of [Eq. \(18\)](#) is given by substituting  $y' = e^{\lambda t}$ . This results in the following quadratic characteristic equation after evaluating the differential terms.

$$M_d \lambda^2 + D_d \lambda + K_d = 0 \quad (19)$$

The solution of the  $\lambda$  is given by

$$\lambda_{1,2} = \frac{-D_d \pm \sqrt{D_d^2 - 4K_d M_d}}{2M_d} \quad (20)$$

based on the initial conditions, the constants  $c_1$  and  $c_2$  are determined for the general solution  $y'_c$ , given as -

$$y'_c = c_1 e^{\lambda_1 t} + c_2 e^{\lambda_2 t} \quad (21)$$

The particular solution  $y'_p$  can be found using the method of undetermined coefficients. Taking  $y' = P$ ,  $\dot{y}' = 0$ ,  $\ddot{y}' = 0$  and substituting in the [Eq. \(16\)](#) gives

$$y'_p = P = \frac{w_e}{K_d} \quad (22)$$

The complete solution is given by  $y'_p + y'_c$ . This completes the derivation of the [Eq. \(14\)](#) from [Eq. \(9\)](#). The above solution can be extended to all the six dimension of the task space.

## Supplementary material

Supplementary material associated with this article can be found, in the online version, at doi:[10.1016/j.rcim.2019.04.010](https://doi.org/10.1016/j.rcim.2019.04.010).

## References

- [1] A.D. Udai, S.K. Saha, A. Dayal, Overlaid orthogonal force oscillations for robot assisted localization and assembly, *ISME J. Mech. Des.* 2 (1) (2019) 09–25.
- [2] E.A. Kirchner, N. Will, M. Simmofiske, L. Manuel, V. Benitez, B. Bongardt, M.M. Krell, S. Kumar, M. Mallwitz, A. Seeland, M. Tabie, H. Woehrle, M. Yüksel, A. Heß, R. Buschfort, F. Kirchner, Recupera-reha: exoskeleton technology with integrated biosignal analysis for sensorimotor rehabilitation, *Transdisziplinäre Konferenz SmartASSIST*, (2016), pp. 504–517.
- [3] D. Kuehn, M. Schilling, T. Stark, L.M. Martin Zenzes, F. Kirchner, 2016 system design and field testing of the hominid robot charlie.
- [4] D. Zhang, Y. Xu, J. Yao, Y. Zhao, Design of a novel 5-DOF hybrid serial-parallel manipulator and theoretical analysis of its parallel part, *Robot. Comput Integr. Manuf.* 53 (2018) 228–239.
- [5] J. Brinker, N. Funk, P. Ingenlath, Y. Takeda, B. Corves, Comparative study of serial-parallel delta robots with full orientation capabilities, *IEEE Robot. Autom. Lett.* 2 (2) (2017) 920–926.
- [6] A. Pashkevich, A. Klimchik, S. Briot, D. Chablat, *Performance Evaluation of Parallel Manipulators for Milling Application Global Product Development*, Springer Berlin Heidelberg, 2011, pp. 619–629.
- [7] S. Briot, A. Pashkevich, D. Chablat, Optimal technology-oriented design of parallel robots for high-speed machining applications, *IEEE International Conference on Robotics and Automation*, pp. 1155–1161, 2010.
- [8] M. Z., P. A., A. M., H. G., S. H., Design and control of an end-effector for industrial finishing applications, *Robot. Comput Integr. Manuf.* 53 (2018) 240–253. 2018
- [9] S. Haddadin, Towards Safe Robots- Approaching Asimov's 1<sup>st</sup> law, (2014) Doctoral dissertation. Available from
- [10] H. Huang, B. Li, Z. Deng, Y. Hu, A 6-DOF adaptive parallel manipulator with large tilting capacity, *Robot. Comput Integr. Manuf.* 28 (2) (2012) 275–283.
- [11] C. A., P. R., C. A., L. A., F. P., Collaborative manufacturing with physical human robot interaction, *Robot. Comput Integr. Manuf.* 40 (2016) 1–13.
- [12] A.D. Udai, R.P. Joshi, S.K. Saha, Depth-based localization for robotic peg-in-tube assembly, *International Conference on Intelligent Robots and Systems (IROS 2015)*,

- (2015), pp. 3538–3543.
- [13] M.H. Ang Jr., W. Wang, R.N.K. Loh, T.S. Low, Passive compliance from robot limbs and its usefulness in robotic automation, *J. Intell. Robot. Syst.* 20 (1) (1997) 1–21.
- [14] A.D. Uda, D.H. Salunkhe, A. Dutta, S. Mukherjee, Force/position control of 3 dof delta manipulator with voice coil actuator, Proceedings of the Advances in Robotics. AIR '17, ACM, New York, NY, USA, 2017. 33:1–33:7
- [15] S. Haddadin, M. Suppa, S. Fuchs, T. Bodenmüller, A. Albu-Schäffer, G. Hirzinger, Towards the robotic co-worker, in: C. Pradalier, R. Siegwart, G. Hirzinger (Eds.), *Robotics Research*, Springer Berlin Heidelberg, Berlin, Heidelberg, 2011, pp. 261–282.
- [16] R. Bischoff, et al., The KUKA-DLR lightweight robot arm - a new reference platform for robotics research and manufacturing, *ISR 2010* (41st International Symposium on Robotics) and *ROBOTIK 2010* (6th German Conference on Robotics), Munich, Germany, (2010), pp. 1–8.
- [17] A.D. Luca, A. Albu-Schäffer, S. Haddadin, G. Hirzinger, Collision detection and safe reaction with the dlr-iii lightweight manipulator arm, 2006 IEEE/RSJ International Conference on Intelligent Robots and Systems, (2006), pp. 1623–1630.
- [18] A. Luca A. D., R. Mattone, Sensorless robot collision detection and hybrid force/motion control, Proceedings of the 2005 IEEE International Conference on Robotics and Automation, (2005), pp. 999–1004.
- [19] S. Lee, M. Kim, J. Song, Sensorless collision detection for safe human-robot collaboration, 2015 IEEE/RSJ International Conference on Intelligent Robots and Systems (IROS), (2015), pp. 2392–2397.
- [20] D.S. Lee, J. bok. S., Sensorless collision detection based on friction model for a robot manipulator, *Int. J. Precis. Eng. Manuf.* 7 (2016) 11–17.
- [21] M. Takaiwa, T. Noritsugu, Development of compliance displaying device using pneumatic parallel manipulator, *SICE 2003 Annual Conference (IEEE Cat. No.03TH8734)*, 1 (2003), pp. 492–497.
- [22] C. Stoeffler, S. Kumar, H. Peters, O. Brueels, A. Mueller, F. Kirchner, Conceptual design of a variable stiffness mechanism in a humanoid ankle using parallel redundant actuation, 2018 IEEE-RAS 18th International Conference on Humanoid Robots (Humanoids), (2018).
- [23] Q. Liang, D. Zhang, Z. Chi, Q. Song, Y. Ge, Y. Ge, Six-dof micro-manipulator based on compliant parallel mechanism with integrated force sensor, *Robot. Comput. Integr. Manuf.* 27 (1) (2011) 124–134.
- [24] Y. Qin, K. Zhang, J. Li, J.S. Dai, Modelling and analysis of a rigid compliant parallel mechanism, *Robot. Comput. Integr. Manuf.* 29 (4) (2013) 33–40.
- [25] X. Song, Y. Pan, Y. Chen, Development of a low-cost parallel kinematic machine for multidirectional additive manufacturing, *J. Manuf. Sci. Eng.* (137) (2015) 124–134.
- [26] J. Wu, Y. Gao, B. Zhang, L. Wang, Workspace and dynamic performance evaluation of the parallel manipulators in a spray-painting equipment, *Robot. Comput. Integr. Manuf.* 44 (2017) 199–207.
- [27] A.D. Uda, A.A. Hayat, S.K. Saha, Parallel active/passive force control of industrial robots with joint compliance, 2014 IEEE/RSJ International Conference on Intelligent Robots and Systems, (2014), pp. 4511–4516.
- [28] S. Kumar, B. Bongardt, M. Simnofske, F. Kirchner, Design and kinematic analysis of the novel almost spherical parallel mechanism active ankle, *J. Intell. Robot. Syst.* (2018).
- [29] S. Kumar, H. Woehrle, M. Trampler, M. Simnofske, H. Peters, M. Mallwitz, E.A. Kirchner, Modular design and decentralized control of the recuperative exoskeleton for stroke rehabilitation, *Appl. Sci.* 9 (2019) 626.
- [30] D. Chakarov, Study of the passive compliance of parallel manipulators, *Mech. Mach. Theory* 34 (3) (1999) 373–389.
- [31] J.P. Merlet, Force-feedback control of parallel manipulators, Proceedings. 1988 IEEE International Conference on Robotics and Automation, 3 (1988), pp. 1484–1489.
- [32] D. Stewart, A platform with six degrees of freedom, *Proc. Inst. Mech. Eng.* 180 (1) (1965) 371–386.
- [33] V.E. Gough, S. Whitehall, Universal tyre test machine, Proceedings of 9th International Congress FISITA, (1962). Pp: 117–137
- [34] F. Pierrot, M. Uchiyama, P. Dauchez, A. Fournier, A new design of a 6-dof parallel robot, *JRM* 2 (1990) 308–315.
- [35] N. Zhang, P. Huang, Q. Li, Modeling, design and experiment of a remote-center-of-motion parallel manipulator for needle insertion, *Robot. Comput. Integr. Manuf.* 50 (2018) 193–202.
- [36] G. Wu, S. Bai, Design and kinematic analysis of a 3-RRR spherical parallel manipulator reconfigured with four bar linkages, *Robot. Comput. Integr. Manuf.* 56 (2019) 55–65.
- [37] S. S., Dynamics of the 6-6 stewart parallel manipulator, *Robot. Comput. Integr. Manuf.* 27 (1) (2011) 212–220.
- [38] K.H. Hunt, Structural kinematics of in-parallel-actuated robot-arms, *J. Mech. Transm. Autom. Des.* 105 (4) (1983) 705–712.
- [39] V. Zamanov, Z. Sotirov, Structures and kinematics of parallel topology manipulating systems, *Proc. Int. Symp. on Design and Synthesis*, (1984), pp. 453–458.
- [40] E. Mirshekari, A. Ghanbarzadeh, K.H. Shirazia, Structure comparison and optimal design of 6-rus parallel manipulator based on kinematic and dynamic performances, *Latin Am. J. Solids Struct.* 13 (2016) 2414–2438. 12
- [41] R. Featherstone, *Rigid Body Dynamics Algorithms*, Place of Publication Springer, 2008.
- [42] S. Kumar, M. Simnofske, M. Bongardt B., Integrating mimic joints into dynamics algorithms: exemplified by the hybrid recuperative exoskeleton, *Proceedings of the Advances in Robotics*, (2017), 27:1–27:6
- [43] M.L. Felis, Rbdl: an efficient rigid-body dynamics library using recursive algorithms, *Auton. Robots* 41 (2) (2017) 495–511.
- [44] A.D. Uda, Force control of industrial robots, 2016.
- [45] G. Zeng, A. Hemami, An overview of robot force control, *Robotica* 15 (5) (1997) 473–482.
- [46] B. Siciliano, V. Luigi, From indirect to direct force control: a roadmap for enhanced industrial robots, 2000, 01.
- [47] A.M. Lopes, F.G. Almeida, Acceleration based force-impedance control of a 6-dof parallel robotic manipulator, 2006 IEEE International Conference on Computational Cybernetics, (2006), pp. 1–6.
- [48] S. Haddadin, A. Schaffer, A. Luca De, G. Hirzinger, Collision detection and reaction: a contribution to safe physical human-robot interaction, IEEE/RSJ International Conference on Intelligent Robots and Systems, (2008), pp. 3356–3363.
- [49] M. Geravand, F. Flacco, A. Luca De, Human-robot physical interaction and collaboration using an industrial robot with a closed control architecture, *IEEE International Conference on Robotics and Automation*, Karlsruhe, D, (2013), pp. 4000–4007.
- [50] S. Mohan, B. Corves, Inverse dynamics and trajectory tracking control of a new six degrees of freedom spatial 3-RPRS parallel manipulator, *Mech. Sci.* 8 (2017) 235–248.
- [51] L. Roveda, N. Iannacci, F. Vicentini, N. Pedrocchi, F. Braghin, L.M. Tosatti, Optimal impedance force-tracking control design with impact formulation for interaction tasks, *IEEE Robot. Autom. Lett.* 1 (1) (2016) 130–136.
- [52] L. Roveda, N. Iannacci, L.M. Tosatti, Discrete-time formulation for optimal impact control in interaction tasks, *J. Intell. Robot. Syst.* (2018) 1–11.
- [53] M.S. Branicky, Multiple Lyapunov functions and other analysis tools for switched and hybrid systems, *IEEE Trans Autom Control* 43 (4) (1998) 475–482.
- [54] Bertec multi axial force feedback system. <https://bertec.com/uploads/pdfs/manuals/Force%20Plate%20Manual.pdf>, accessed: 2018-06-26.
- [55] A. Arimoto, S. t stability and robustness of PID feedback control for robot manipulators of sensory capability j robotics research, 1st Int. Symp. Journal Article, MIT Press, 1984, pp. 783–799. <https://ci.nii.ac.jp/naid/80014492902/en/>
- [56] Vicon motion capture system. <https://www.vicon.com/file/vicon/viconstandard2017editions.pdf>, accessed: 2018-06-26.
- [57] Dynamixel MX-64t motors. [http://support.robolit.com/en/product/actuator/dynamixel\\_mx\\_series\\_mx-64at\\_ar.html](http://support.robolit.com/en/product/actuator/dynamixel_mx_series_mx-64at_ar.html), accessed: 2018-06-26.